SLAC–PUB–10037
July 1995

QCD at SLD*

R.J. Plano
Rutgers University, New Brunswick, NJ 08903

Representing the SLD Collaboration

Invited talk presented at 23rd Annual SLAC Summer Institute on Particle Physics: The Top Quark and the Electroweak Interaction

Stanford, California

July 10 – July 21, 1995

* Work supported in part by Department of Energy contract DE–AC03–76SF00515.

QCD AT SLD

Richard Plano*
Rutgers University
New Brunswick, NJ 08903
Representing the SLD Collaboration

ABSTRACT

This talk reviews seven SLD papers, which provide useful, unique, and precise contributions to our understanding of hadron production in the decay of Z^0's produced in e^+e^- collisions. The data were gathered by the SLAC Large Detector (SLD) at the SLAC Linear Collider (SLC). This accelerator/detector is able to compete with LEP in many studies, in spite of smaller statistics, due to systematic advantages including a tiny and stable interaction region combined with a precise high-resolution vertex detector, excellent particle identification, and a highly polarized electron beam.

The papers include studies of:

- factorial and cumulant moments,[1]
- charged multiplicities produced by b, c, and uds quarks,[2]
- rapidity gaps,[3]
- orientations and energy partitions of three-jet events,[4]
- jet handedness,[5]
- triple-product correlation in polarized Z^0decays to three jets,[6] and
- $\pi^{\pm}$, $K^{\pm}$, p, K^0, and Λ production in Z^0 decays.[7]

Comparisons are made to LEP results where appropriate.

*Supported by NSF Grant PHY-9510439.

1 Introduction

Quantum Chromodynamics (QCD), the local non-Abelian gauge field theory of quarks and gluons, is now reasonably well-understood and capable of making many testable predictions. The reaction which is discussed here,

$$e^+e^- \to Z^0 \to q\bar{q} \;\; (g)\cdots \to hadrons, \;\; e.g., \;\; \pi K p \rho \phi \Delta \Lambda b \cdots \quad , \tag{1}$$

is illustrated schematically in Fig. 1. The production of $q\bar{q}$ by e^+e^- annihilation via Z^0 exchange is well-understood; γ exchange is almost negligible—about 1100 times less probable than Z^0 exchange. The resulting "parton showers" [Fig. 1 (i)] as gluons and further $q\bar{q}$ pairs are produced: can be calculated using perturbative QCD (PQCD), for example, in the Modified Leading Logarithm Approximation. Next [Fig. 1 (ii)], the partons hadronize in a manner which is not fully understood. The assumption of Local Parton-Hadron Duality (LPHD), which states that the distributions of final state particles are related in some detail to the original partons, is the source of numerous predictions, some of which will be tested in this paper. The physical hadrons [Fig. 1 (iii)] produced by the hadronization process are often unstable and decay into the final state particles [Fig. 1 (iv)] which are observed by the detector. While these decays are well-understood, they add a considerable complication to the analysis.

Numerous properties of the final state particles can be measured and used to provide information about the reaction that produced them. The SLD at the SLC is well-equipped to contribute to these investigations.

2 Features of SLD

A cross section of one quarter of the SLD detector is shown in Fig. 2 and an isometric view in Fig. 3. The characteristics of this detector which are most important for the results presented here will be briefly described. See the original design report[8] for details.

The position of the Interaction Point (IP) at which the e^+e^- collision takes place is constrained by the beam size to lie within a region roughly 0.8 μm vertically, 2.6 μm horizontally ("flat" beams), and 700 μm along the beam. The transverse position of the collision region is quite stable, with variations typically less than 10 μm over periods of a few hours. To determine the transverse position

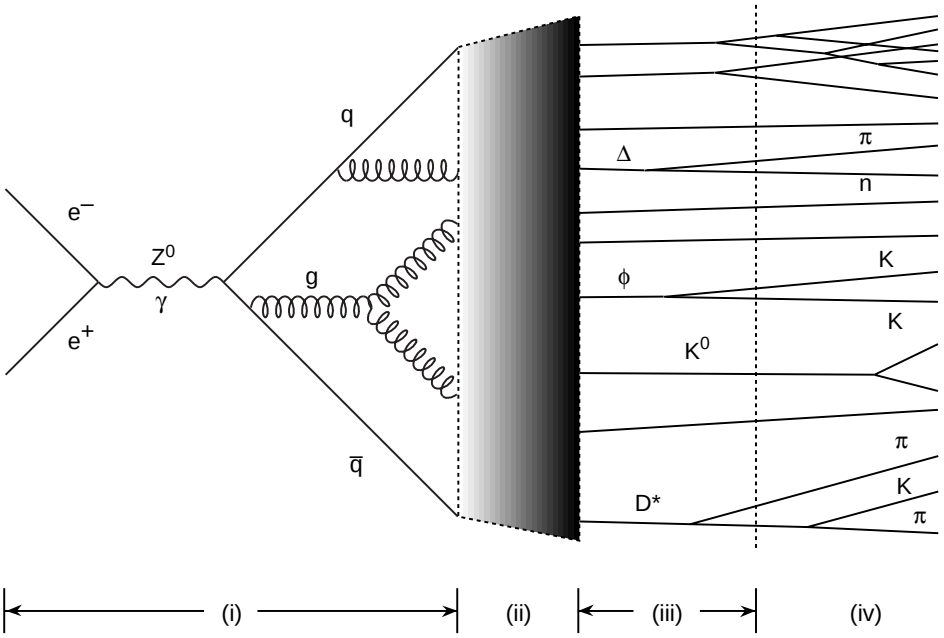

Fig. 1. QCD description of $e^+e^- \to Z^0 \to q\bar{q}g \cdots \to$ hadrons.

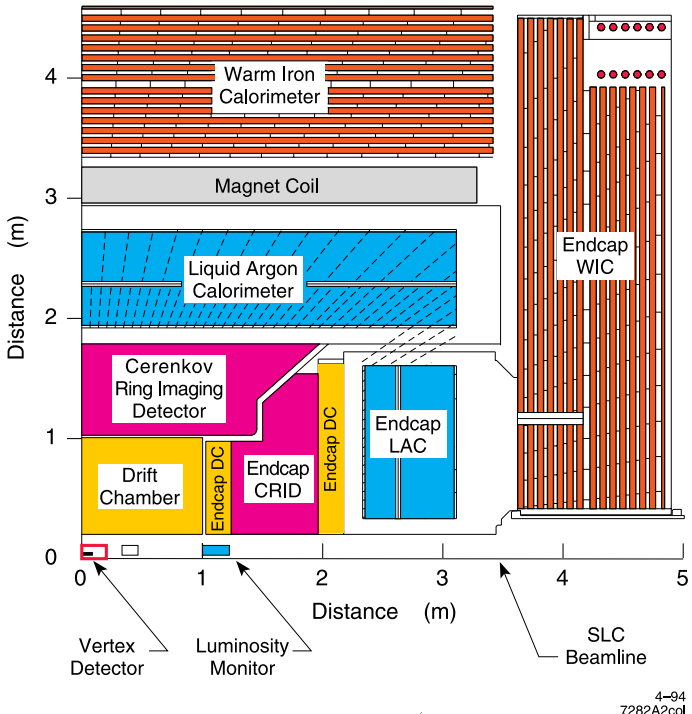

Fig. 2. The SLD detector (quadrant view).

accurately, the intersection point of tracks from hadronic events is averaged over about 30 successive hadronic events. Poor quality tracks are discarded, leaving about 300 tracks in each fit, constraining the IP to less than 10 μm.

The vertex detector (VXD) consists of 120 million pixels, each 22 μm $\times$ 22 μm, placed in three layers between 2.9 cm and 4.2 cm radius around the beamline. The VXD has a point resolution of about 5 μm in the plane perpendicular to the beamline.

The Central Drift Chamber (CDC) has 80 layers of sense wires roughly parallel to the beamline with 48 layers which are at angles of $\pm$ 50 mrad to provide stereo information. The intrinsic accuracy of a hit in the CDC, which tells the distance of a track from a wire, is 85 μm near the center of a drift cell.

Combining the VXD and the CDC provides an impact parameter resolution (distance of closest approach of a track to the IP) of (p_t in GeV/c):

$$\sigma_{r\phi} = \frac{76\mu m}{p_t\sqrt{sin\theta}} \bigoplus 11\mu m \tag{2}$$

and, using the magnetic field of 6 kG parallel to the beam, a momentum resolution of:

$$\frac{\sigma_{p_t}}{p_t} \sim 0.5\% p_t \bigoplus 1.0\%. \tag{3}$$

The Cherenkov Ring Imaging Detector (CRID) uses Cherenkov radiation to measure the speed of charged particles which, when combined with a momentum determination, identifies the particle. The CRID[9] will be described in detail later in this talk.

The Liquid Argon Calorimeter (LAC) and Warm Iron Calorimeter (WIC) together serve both as an electromagnetic calorimeter with an energy resolution of 15% at 1 GeV and an angular resolution of a few milliradians, and a hadronic calorimeter with an energy resolution of 55% at 1 GeV.

Rather than describe in detail the criteria used for event triggers, track selection, and event selection for each analysis, typical values are listed here; in no case do the results depend sensitively on the details.

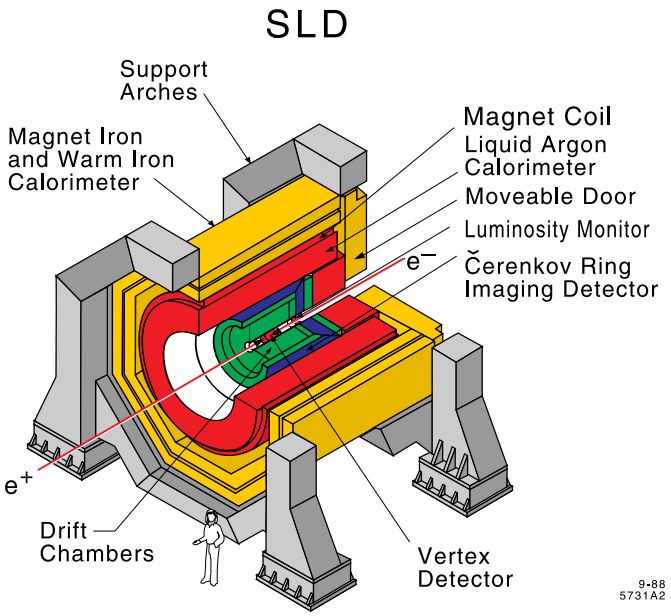

Fig. 3. The SLD detector (isometric view). The end caps have been removed for clarity.

Typical Event Trigger: an event is recorded if it passes any of the following criteria:

1. $E_{LAC} > 12$ GeV,
2. ≥ 2 tracks reconstructed in the CDC, using only the cell locations, and
3. $E_{LAC} > 4$ GeV and ≥ 1 CDC track.

Once a trigger is selected, tracks are reconstructed in the CDC and VXD. A track is selected if it passes all of:

1. $DOCA_{\perp} < 5$ cm, $DOCA_{\parallel} < 10$ cm, $\perp \equiv$ perpendicular to the beam,
2. $\mid cos\theta_{trk} \mid < 0.80$ $(37^{\circ} < \theta_{trk} < 143^{\circ})$, and
3. $p_{\perp} = p \sin\theta_{trk} > 0.15$ GeV/c.

$DOCA$ is the Distance Of Closest Approach of the extrapolated track to the IP. θ_{trk} is the track angle relative to the beam. An event is selected for further analysis if the following criteria are all met:

1. ≥ 5 selected tracks,
2. $\mid cos\theta_T \mid < 0.71 \quad (44.8^{\circ} < \theta_T < 135.2^{\circ})$, and
3. $E_{vis} > 20$ GeV, using the tracks selected above.

θ_T is the angle between the thrust axis of the event and the electron beam direction; E_{vis} is the energy calculated from the momentum measured in the CDC assuming the pion mass for all tracks.

3 Charged Multiplicity

The first two papers[1,2] concern different aspects of charged multiplicity, the detailed shape of the overall charged multiplicity distribution, and the dependence of average multiplicities on the flavor of the primary $q\overline{q}$ pair.

Multiplicity distributions contain fundamental information about interactions and have often been studied.[10] The first guess—a Poisson distribution based on stochastic processes—works very badly, as it predicts that the fractional width should decrease as the multiplicity increases. "KNO scaling,"[11] which postulates that the multiplicity distribution is a universal function of $n/ < n >$ and so predicts a constant fractional width, does much better, but also fails at the highest energies.

"Factorial and cumulant moments in $e^+e^- \to$ hadrons at the Z^0 resonance"[1] follows a proposal of I. M. Dremin[12] to make a sensitive test of the shape of the overall multiplicity distribution. This is the first study of H_q, the ratio of the cumulant moment K_q to the factorial moment F_q:

$$H_q = K_q/F_q; \qquad F_q = \frac{< n(n-1)\cdots(n-q+1) >}{< n >^q} = \sum_{m=0}^{q-1} C_{q-1}^m K_{q-m} F_m. \qquad (4)$$

C_{q-1}^m are the binomial coefficients, and $F_0 = F_1 = K_1 = 1$. H_q is predicted to have the following behavior for the indicated models of particle production.

Poisson	NBD	DLA	NLA	NNLA
0	q^{-k} $k \approx 24$	q^{-2}	Minimum at $q \approx 5$	Mininum at $q \approx 5$, then oscillates

In this table, NBD is the Negative Binomial Distribution, DLA refers to a QCD calculation done in leading order (Double Logarithmic Approximation), and NLA, NNLA refer to Next-to-Leading and Next-to-Next-to Leading Approximation QCD calculations. These calculations[12,14] illustrate the striking sensitivity of H_q to models whose predictions look quite similar when plotted as simple multiplicity distributions.

Monte Carlo (MC) calculations, including a detailed description of the SLD detector, were used to correct for effects introduced by geometrical acceptance and resolution, γ conversions, and particle interactions. Charged decay products of particles with lifetimes $< 3 \times 10^{-10}$ s were included in the multiplicity count.

Figure 4 shows the data with a fit to a NBD distribution. Although the fit is quite good ($k = 24.9 \pm 0.9, < n > = 20.6 \pm 0.1, \chi^2/NDF = 22.9/24$), note that all the measured points for $n \geq 36$ are **above** the fitted curve.

Figure 5 shows the H_q obtained from these data (points with error bars). Also shown are lines connecting H_q values calculated from the Poisson (dots) and NBD (dashes) distributions fitted to the multiplicity distribution. The Poisson distribution, which is identically zero, is unacceptable at $q \leq 3$ and, as is especially clear from the magnified view in the inset, NBD is also very poor. Interestingly, an analysis[14] of the multiplicity distribution observed by UA5 in $\overline{p}p$ interactions at 546 GeV shows very similar behavior of H_q, including the oscillations. MC

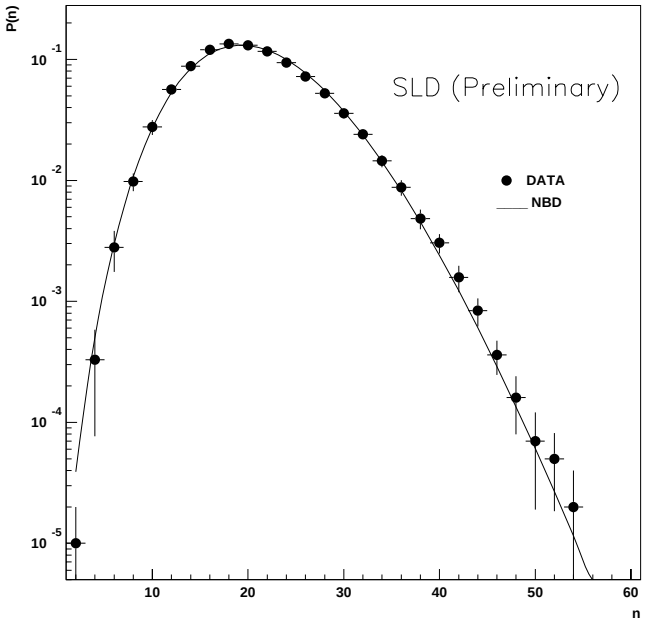

Fig. 4. Negative Binomial Distribution fit to the multiplicity distribution.

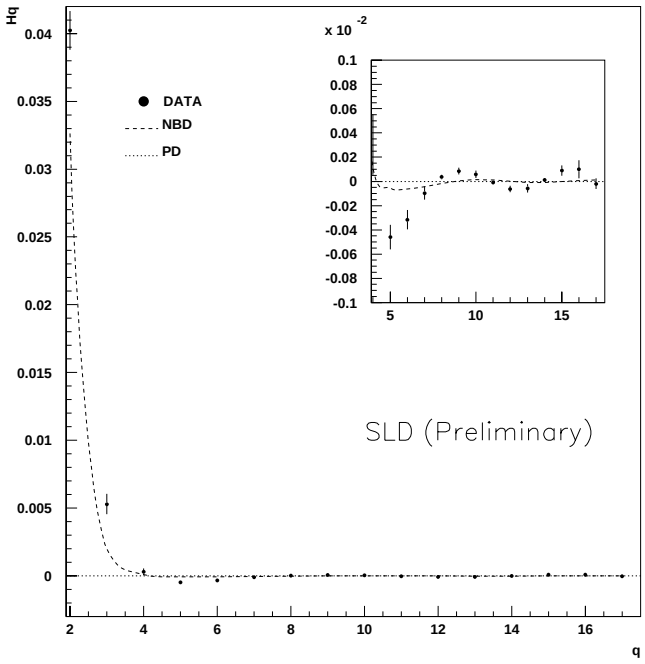

Fig. 5. H_q fit to data compared to NBD and Poisson predictions. Note enlarged view in inset.

calculations of the SLD data have shown that the oscillations in H_q are not related to the effective truncation at high multiplicity due to the finite size of the data sample.

Higher order calculations,[13] including the NNLA, describe the shape of the H_q distribution rather well. These results tend to support both the validity of QCD at the parton level and the concept of LPHD—the idea that the observable final state distributions reflect in some detail the distributions of the underlying partons.

"Measurement of the charged multiplicities of b, c, and light quark events from Z^0 events"[2] tests how the **average** multiplicities depend on flavor.

To obtain uds, b, and c quark enriched samples without bias, divide each event into two hemispheres by a plane perpendicular to the thrust axis. Then:

- Tag each hemisphere as described below.

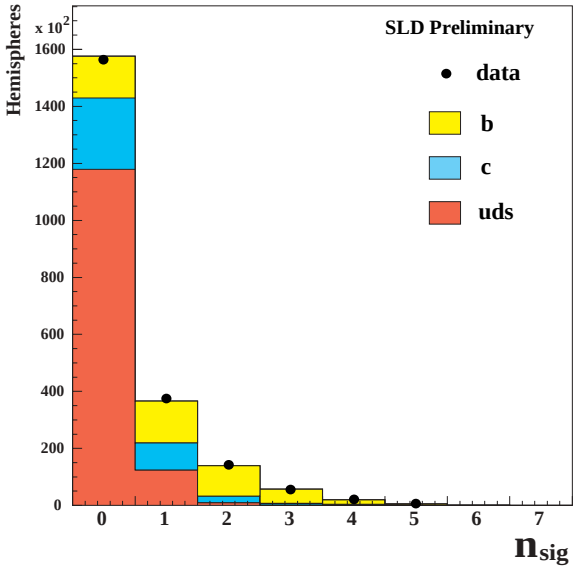

Fig. 6. MC estimates of the uds, b, and c components of hemispheres *vs.* n_{sig} and data *vs.* n_{sig}.

- Use the tag to label the **opposite** hemisphere; this is necessary to avoid bias.
- Double the count in the labeled hemisphere.

uds and b tags are based on n_{sig}, the number of tracks in a hemisphere with significant impact parameters, b, where $b/\sigma_b > 3$. The c quark tag is based on detection of a D^+ or D^{*+}. The tags, the resulting number of hemispheres tagged, and the purity of the tags are summarized in the table.

Quark	Tag	Purity	# Hemispheres
uds	$n_{sig} = 0$	75%	156K
b	$n_{sig} \geq 3$	94%	8.5K
c	$D^+ or D^{*+}$	58%	1.2K

Figure 6 shows the number of hemispheres containing n_{sig} significant tracks in the data. The shaded bars indicate MC estimates of the quark content of each n_{sig} bin. The MC is in good agreement with the data and gives estimates of the purity provided by the n_{sig} cuts.

The counts in the labeled hemispheres are then used to form $\overline{n}_{uds}$, $\overline{n}_b$, and $\overline{n}_c$, as well as $\delta\overline{n}_b = \overline{n}_b - \overline{n}_{uds}$ and $\delta\overline{n}_c = \overline{n}_c - \overline{n}_{uds}$.

Perturbative QCD (PQCD) in the modified leading logarithm approximation (MLLA) predicts[15] that $\delta\overline{n}_b = \overline{n}_b - \overline{n}_{uds}$ and $\delta\overline{n}_c = \overline{n}_c - \overline{n}_{uds}$ are independent

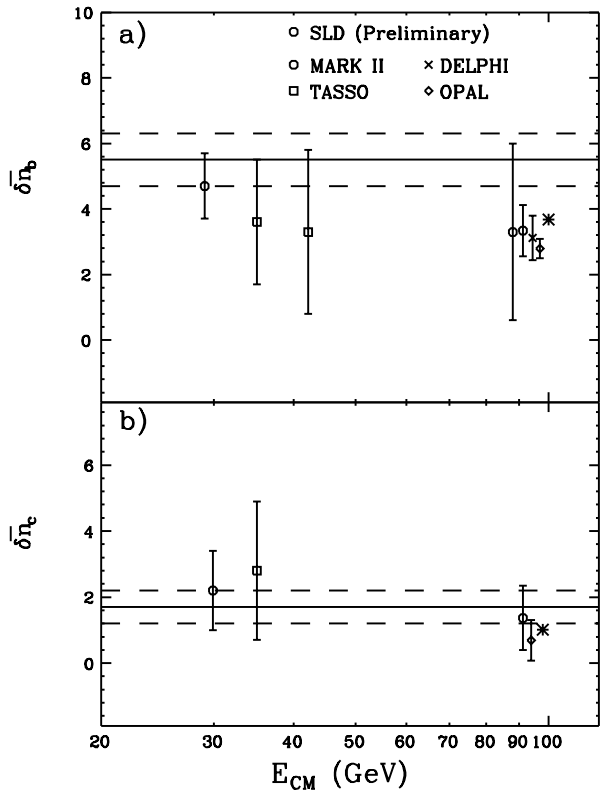

Fig. 7. $\delta\overline{n}_b = \overline{n}_b - \overline{n}_{uds}$ and $\delta\overline{n}_c = \overline{n}_c - \overline{n}_{uds}$ as a function of the center-of-mass energy. The solid lines are MLLA QCD + LPHD predictions with uncertainties indicated by the dashed lines. The stars indicate another prediction (see text).

of energy within about 0.1 track. Furthermore, MLLA QCD + LPHD[15] and an alternative approach[16] have made definite predictions which are summarized in the table and in Fig. 7.

Ref.	These data	Ref. 15	Ref. 16
$\delta\overline{n}_b$	3.34 ± 0.13	5.5 ± 0.8	3.68
$\delta\overline{n}_c$	1.37 ± 0.45	1.7 ± 0.5	1.01

The data are in reasonable agreement with the predictions within the rather large errors. As shown in Fig. 7, DELPHI and OPAL are in good agreement with the SLD numbers. Furthermore, data at lower energies from MARK II and TASSO are consistent with negligible energy dependence as predicted.

4 A Study of Rapidity Gaps

Events containing large rapidity gaps have been reported at HERA and at Fermilab, where they have been interpreted as evidence for the Pomeron.[17,18] Hadronic events from e^+e^- annihilation containing large rapidity gaps produced by a color-screening mechanism are expected to occur at a very small rate.[19] This is the **first** study of rapidity gaps in e^+e^- annihilations, and it will be useful for the analysis of the Fermilab/HERA data, since the Pomeron is not expected in e^+e^- annihilations.

Figure 8 summarizes the results obtained in this measurement.[3] Figure 8(a) shows the inclusive rapidity distribution of charged tracks in hadronic events, Fig. 8(b) the average gap (average difference in rapidity between neighboring charged tracks), and Fig. 8(c) the distribution of the largest gap in each event. As can be seen most clearly in Fig. 8(c), there are many more large gaps than are predicted by the hadronic MC. However, when contamination from $\tau^+\tau^-$ events in the hadronic sample are included in the MC, the disagreement disappears.

This data then provides natural spectra for gap distributions which are needed for the analysis of gap distributions found in hadronic events.

5 Orientation and Energy Partition of Three-Jet Events

Three-jet events have been studied since 1979 (Ref. 20) when they were used to support the existence of a spin 1 gluon produced in the reaction $e^+e^- \to Z^0 \to q\overline{q}g$. Similar events measured in the SLD detector have been analyzed in terms of the energies and orientation angles of the three jets.[4]

The Liquid Argon Calorimeter (LAC), which covers 98% of the solid angle, was used for this analysis as it measures the jet energies and angles with good precision. The events are analyzed by ordering the three jets by their energy in the overall center of mass: $E_1 > E_2 > E_3$. Then the Ellis-Karliner angle is formed:

$$\cos\theta_{EK} = \frac{x_2 - x_3}{x_1}; \qquad x_i = 2E_i/\sqrt{s}. \tag{5}$$

Distributions of these quantities are shown in Fig. 9. These plots show the data, fully corrected to the parton level, as dots and compare the data with

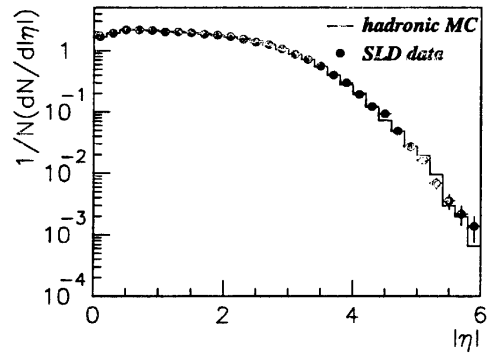

Fig 1a

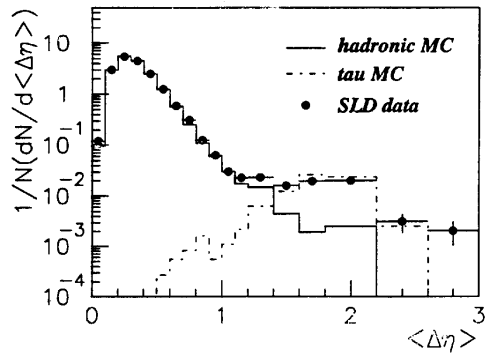

Fig 1b

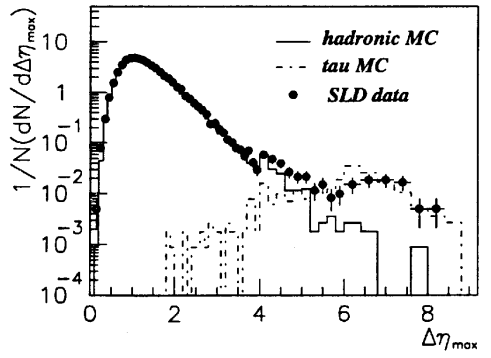

Fig 1c

Fig. 8. The (a) rapidity distribution, (b) average gap distribution, and (c) maximum gap distribution. A hadronic MC with a 0.3% $\tau^+\tau^-$ contamination provides an excellent description.

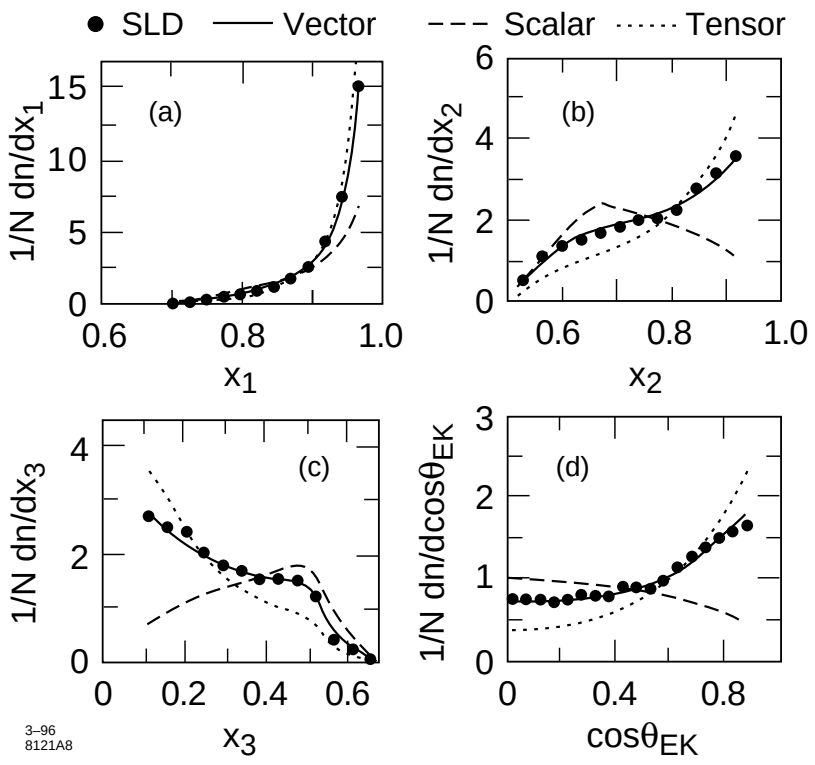

Fig. 9. Fully corrected data from this experiment are shown as dots; leading-order predictions are shown as solid lines for the vector case, dashes for scalar, and dots for tensor.

leading-order predictions assuming vector, scalar, and tensor gluons. The agreement of the data with the predictions for a vector gluon is in all cases satisfactory. Scalar and tensor fits are very poor and appear to be excluded, but precise limits are not feasible without $O(\alpha_s^3)$ calculations.

6 Jet Handedness

The polarized beam carries with it an obvious handedness. It is not unreasonable to expect that the high polarization of the electron beam might carry over into measurable final state effects. Since there is no complete theory of hadronization and very few measurements of any spin-dependent quantities, this is a fertile area for experimental studies.

The final three papers reported here[5–7] address three specific spin-dependent questions:

- Jet handedness. $\Omega = \vec{t} \cdot (\vec{k}_1 \times \vec{k}_2)$ to measure spin along the jet axis, $\vec{t}$, using the momenta of two particles in the jet, chosen to be sensitive to handedness.
- The triple product $\vec{S}_Z \cdot (\vec{k}_1 \times \vec{k}_2)$, where $\vec{k}_1$, $\vec{k}_2$ are the momenta of the highest and second-highest energy jets.
- A search for a leading particle effect to observe $\vec{S}_Z \cdot \vec{p}$, where $\vec{p}$ is the momentum of a particle composed of quarks.

SLC/SLD is an ideal place to study asymmetries in Z^0 decay as the beam polarization assures that the partons from Z^0 decay are highly longitudinally polarized. If techniques to observe this polarization could be developed, the spin dynamics of a variety of hard processes could be studied.

The polarization of the Z^0, A_Z, is related to the polarization of the beam electron, P_{e^-}, by:

$$A_Z = \frac{P_{e^-} - A_e}{1 - P_{e^-} A_e}; \qquad A_f = \frac{2 v_f a_f}{v_f^2 + a_f^2}, \tag{6}$$

where v_f, a_f are the vector and axial vector couplings of fermion f to the Z^0; $A_e \approx 0.16$. The following table shows how the large beam polarization at the SLC produces large forward-backward asymmetries A_{FB} for both u and d quarks, as well as highly polarized forward/backward quarks.

P_{e^-}	A_Z	A_{FB}(u-type)	A_{FB}(d-type)	$P_q(\cos\theta = \pm 1)$
+0.77	+0.70	-0.35	-0.49	$\pm$ 0.70
-0.77	-0.83	+0.42	+0.58	$\mp$ 0.83

By contrast, the Z^0 polarization at LEP, where the beams are unpolarized, is only 0.16. So the SLC errors, both statistical and systematic, are reduced by a factor close to five. This reduction in the statistical error could be compensated at LEP by an increase in the number of events by a factor of about 25; it is not possible to reduce the systematic errors by any simple technique.

Further, the ability to reverse the sign of the polarization is an extremely important aid in the further reduction of systematic errors at SLAC. It can be used to prove that an observed asymmetry is not due to an asymmetry in the detector or in the analysis.

"An improved limit on jet handedness in Z^0 decays"[5] doubles the sensitivity obtained with the 1993 run of the SLD detector.[21] The increased accuracy is due

both to the increased statistics and the higher polarization, which increased, on average, from 0.63 to 0.78, equivalent to a 50% increase in statistics.

Two observables were chosen to study polarization along a jet axis, one based on the magnitude of the momenta and the other on the charge of the particles. $\Omega_{hel} = \hat{t} \cdot (\vec{k_1} \times \vec{k_2})$, where $k_1 > k_2$ and $\hat{t}$ is pointing along the jet axis, has the same transformation properties as the "helicity-based" polarization:

$$P^f_{hel}(\cos\theta) \equiv \frac{\sigma^f_R + \sigma^{\overline{f}}_R - \sigma^f_L - \sigma^{\overline{f}}_L}{\sigma^f_R + \sigma^{\overline{f}}_R + \sigma^f_L + \sigma^{\overline{f}}_L} = 2\frac{A_Z \cos\theta}{1+\cos^2\theta}. \tag{7}$$

$\Omega_{chi} = \hat{t} \cdot (\vec{k_+} \times \vec{k_-})$ has the transformation properties of the "chirality-based" polarization:

$$P^f_{chi} \equiv \frac{\sigma^f_R - \sigma^{\overline{f}}_R - \sigma^f_L + \sigma^{\overline{f}}_L}{\sigma^f_R + \sigma^{\overline{f}}_R + \sigma^f_L + \sigma^{\overline{f}}_L} = -A_f \tag{8}$$

which is independent of $\cos\theta$ and beam polarization. Note that the beam polarization at SLC/SLD allows examination of helicity as well as chirality-based asymmetries; LEP can study only chirality-based asymmetries.

The measure of interest is then:

$$H = \alpha P = \frac{N_{\Omega<0} - N_{\Omega>0}}{N_{\Omega<0} + N_{\Omega>0}} \quad ; \tag{9}$$

H is the jet handedness, shown in Fig. 10. P is the expected polarization of the underlying partons, and α is the analyzing power of the method. The data was broken up into light-flavor jets and heavy-flavor jets using the number of nonzero impact parameters in the opposite hemisphere as described earlier with results given in the table. The numbers in parentheses are the 95% confidence upper limits on the magnitude of the analyzing power.

	Analyzing Power		
Analysis	Light-Flavor Jets	Heavy-Flavor Jets	All Jets
Helicity	$+0.005 \pm 0.017$ (.037)	$+0.025 \pm 0.019$ (.056)	-0.006 ± 0.022 (.047)
Chirality	$+0.017 \pm 0.026$ (.062)	$+0.014 \pm 0.013$ (.035)	$+0.005 \pm 0.017$ (.036)

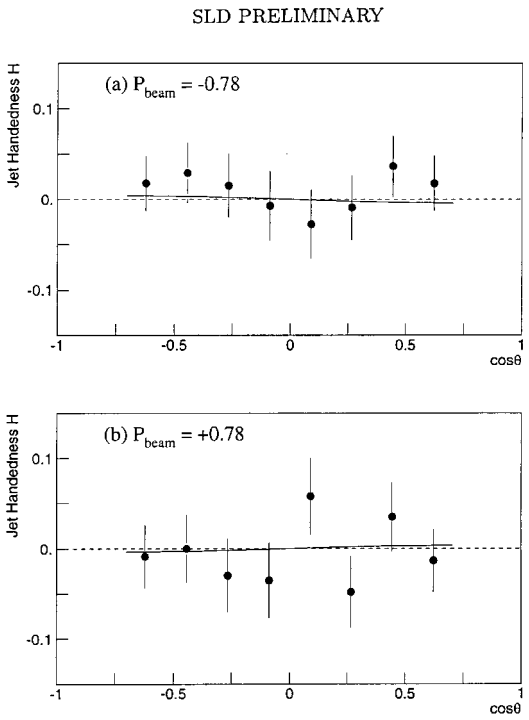

Fig. 10. Simultaneous fits to light-flavor jets for both signs of the electron beam polarization.

7 Triple-Product Correlations in Polarized Z^0 Decays

This is the first measurement of the triple-product correlation in polarized Z^0 decays into three hadronic jets.[6] The CP-even and T-odd triple product $\cos\omega \propto \vec{S_Z} \cdot (\vec{k_1} \times \vec{k_2})$ is sensitive to physics beyond the Standard Model, which predicts unobservably small values. Here, $\vec{S_Z}$ is the Z^0 polarization vector and $\vec{k_1}$, $\vec{k_2}$ are the largest and second-largest jet momenta. $\vec{S_Z}$ is in the direction of the electron beam polarization.

The variable $\cos\omega$ is even under C and P reversals, and odd under T_N, where T_N reverses momenta and spin vectors without exchanging initial and final states. Since that is not a true time-reversal operation, a nonzero value is possible without CPT violation. Though this variable was proposed[22] in 1980 as a means of observing the non-Abelian character of QCD at lower energies, no measurements have been made since a longitudinally polarized electron beam is required, but has not been available until now.

The angular distribution expected after integrating over other variables is[23]:

$$\frac{d\sigma}{d\cos\omega} \propto (1 - \frac{1}{3}\cos^2\omega) + \beta \cdot A_Z \cdot \cos\omega, \tag{10}$$

where ω is the polar angle of the vector along $\vec{k_1} \times \vec{k_2}$, and A_Z is the spin polarization of the Z^0 along the Z axis. Since the sign and magnitude of this term is different for the two beam helicities, the $\cos\omega$ distribution is examined separately for the two cases. It has been shown[23] that in the Standard Model, β vanishes identically at tree level, but could have a nonzero value due to contributions from the interference between tree level and higher-order terms. However, the effect is expected to be very small ($|\beta| < 10^{-5}$). Thus, any experimentally observable nonzero value would indicate physics beyond the Standard Model.

Figure 11 shows the angular distributions for left-handed ($P_{e^-} < 0$) and right-handed ($P_{e^-} > 0$) electron beams for the 1994-1995 data. A fit, also shown in Fig. 11 and including the 1993 data, yields $\beta = 0.008 \pm 0.015$ with 95% confidence level limits of $-0.022 < \beta < 0.039$. These limits take into account the acceptance and efficiency of the detector as well as the probability (76.4%) that the jet-energy ordering mirrors that of the partons.

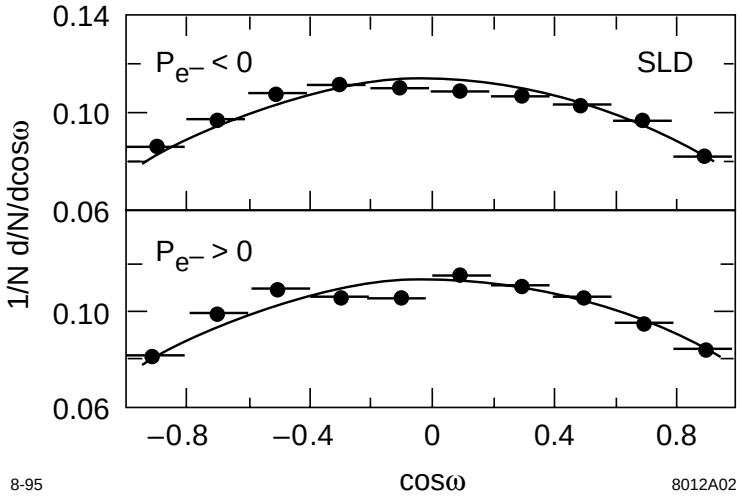

Fig. 11. $\cos\omega$ distribution of the 1994-1995 data for (top) left-handed and (bottom) right-handed electron beams.

Thus, the first measurement of the triple-product correlation in polarized Z^0 decays to three jets finds no statistically convincing asymmetry and sets a 95% confidence level limit on the rate of T_N-odd Z^0 decays to three jets of $|\beta| < 0.039$.

8 Production of $\pi^{\pm}$, $K^{\pm}$, p, K^0, Λ in Hadronic Z^0 Decays

The SLD detector combined with the SLC has a variety of excellent capabilities that are useful for identifying different types of particles; most of them were utilized in the analysis described in this study[7]:

- Charged hadrons can be identified from the cone angle of their Cherenkov radiation in a liquid and/or gas radiator as measured in the CRID (Cherenkov Ring Imaging Detector).
- Light- and heavy-flavor events can be isolated using the impact parameter analysis described earlier using combined drift chamber and vertex detector reconstruction.

- Samples enriched in quark jets or in antiquark jets can be isolated using the electron beam polarization and the fact that quarks (antiquarks) prefer to be left- (right-) handed.

Since it is so vital to this analysis, a short description of the CRID detector is appropriate. Figure 12 illustrates the principal design features of the barrel CRID. A charged particle, whose momentum is determined by the central drift chamber, passes through a liquid radiator producing an average of 11 detected photons. After passing through a drift box, the particle emits an average of nine detected photons in a gas radiator. The gas photons are focused back onto a circular image in the drift box by a set of spherical mirrors; the liquid photons also produce a roughly circular image due to the fact that the liquid radiator is thin compared to its distance from the drift box "proximity focusing." The two radiators with different indices allow particle identification over a wide range of momenta using the fact that the cone angle of the emitted radiation is given by $\cos\theta = 1/n\beta$, where n is the index of refraction and β is the speed of the particle. The number of photons expected is also used in identifying particles as the number increases from zero below threshold to an average of about ten for each of the two radiators for momenta far above threshold. The main properties of the two radiators are shown in the table.

				Max. Ring	Threshold (GeV/c)		
Radiator	Material	Length	Index	Radius	π	K	p
Liquid	C_6F_{14}	1 cm	1.277	16 cm	0.18	0.62	1.2
Gas	C_5F_{12}	$\sim$ 40 cm	1.0017	3 cm	2.4	8.4	16.0

There are altogether 40 drift boxes and 400 mirrors in the barrel CRID. The drift boxes have a small amount of Tetrakis diMethylAmine Ethylene (TMAE) which acts as a photocathode, converting the photons to electrons with a mean free path of around 1.6 cm.

A maximum likelihood is constructed for each mass hypothesis for each track, where the product, i, is over all measured photons. We expect n_j photons at angles θ_j and background b. Particle identification is then based on differences in L_j. For example, $L_K - L_\pi > 4.5$ identifies the particle as a K and rejects the π interpretation with 3σ confidence.

$$\pounds_j \propto -ln\left(\frac{\overline{n_j}}{n!}e^{-\overline{n_j}}\prod_i[exp\left(\frac{-(\theta_i-\theta_j)^2}{2\sigma^2}\right)+b]\right). \qquad (11)$$

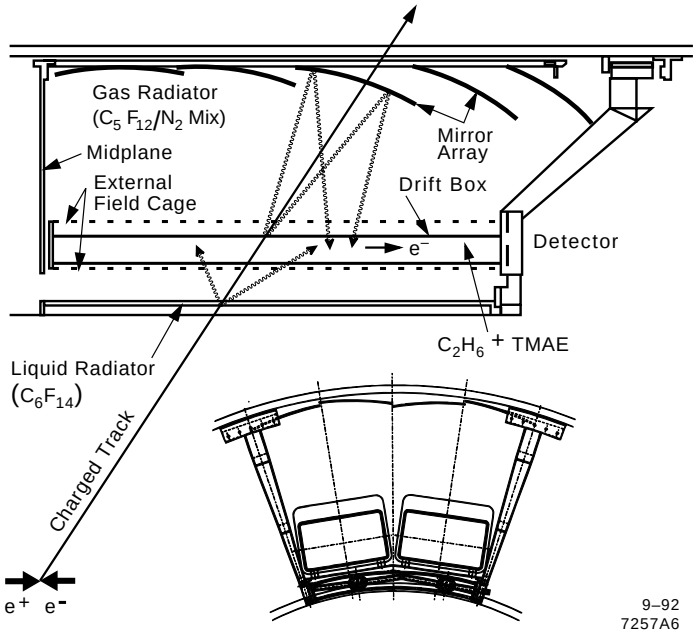
Gas Radiator
($C_5 F_{12}/N_2$ Mix)
Midplane
External
Field Cage
Mirror
Array
Drift Box
Detector
e^-
C_2H_6 + TMAE
Liquid Radiator
(C_6F_{14})
Charged Track
e^+ e^-

9–92
7257A6

$$\begin{pmatrix} f_\pi \\ f_K \\ f_p \end{pmatrix} = \begin{bmatrix} \epsilon_{\pi\pi} & \epsilon_{\pi K} & \epsilon_{\pi p} \\ \epsilon_{K\pi} & \epsilon_{KK} & \epsilon_{Kp} \\ \epsilon_{p\pi} & \epsilon_{pK} & \epsilon_{pp} \end{bmatrix}^{-1} \frac{1}{n_{ch}} \begin{pmatrix} N_\pi \\ N_K \\ N_p \end{pmatrix}.$$

Corrections for electrons and muons, which are sometimes confused with pions, were made using the MC. Only negative tracks are used below 2 GeV/c as an appreciable number of slow protons are produced in secondary interactions.

The efficiencies for identifying particles of type i as type j, where $i, j = \pi, K, p$ are shown in Fig. 13 as a function of momentum. The values at a given momentum from this array of graphs are essentially the efficiency matrix described above. Correct identification efficiencies ($i = j$) peak near 90% and misidentification rates are typically less than 5% with a peak value of 9%. These efficiencies were checked using pions from K^0_s decays with results that agreed with the MC simulation within the statistical errors.

Figure 14 shows the measured hadron fractions as a function of momentum. The solid line and dashed line show predictions of the JETSET 7.4 simulation program,[24] both in the standard version, called "Vanilla" and in the "SLD tuned" version, which includes a better β-decay model and is tuned to better reproduce a wide range of data from LEP. The lower figure shows the sum of the efficiencies. Since the efficiencies were not constrained to add up to 1.0, the consistency of the sum with 1.0 is a check on the validity of the method.

In some momentum regions, it is impossible to distinguish between two of the three species, so the procedure was reduced to a 2 x 2 analysis. In that case, only the fraction of the identified species are shown, i.e., protons in the liquid (gas) analysis above 3 (27) GeV/c and pions in the gas analysis below 10.5 GeV/c. Systematic errors dominate for the liquid points and are comparable to the statistical errors for the gas points.

Pions dominate at low momentum, but decline gradually to two-thirds by 10 GeV/c. Most of the decline is taken up by the kaon fraction, which rises to about one-third, whereas the proton fraction remains below one-tenth. These results are in agreement with results from LEP, where particle identification has been carried out both using ionization[25,26] as shown in Fig. 15 and using ring imaging[27] similar to CRID as shown in Fig. 16. Combining the techniques permits continuous coverage from 0.2 GeV/c to 35 GeV/c.

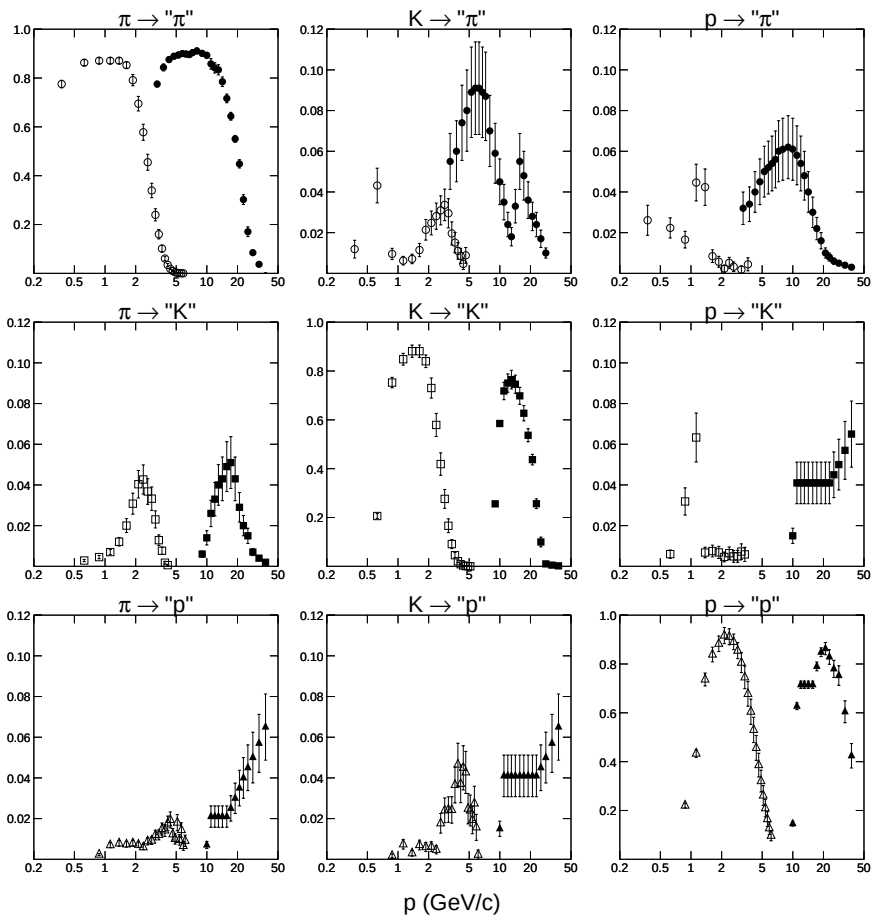

Fig. 13. Identification efficiencies for charged π, K, and $p/\overline{p}$ as a function of momentum for particles identified using the liquid radiator (open circles at lower momenta) and the gaseous radiator (solid circles). The notation $K \rightarrow$ "π" signifies true K's which are misidentified as π's.

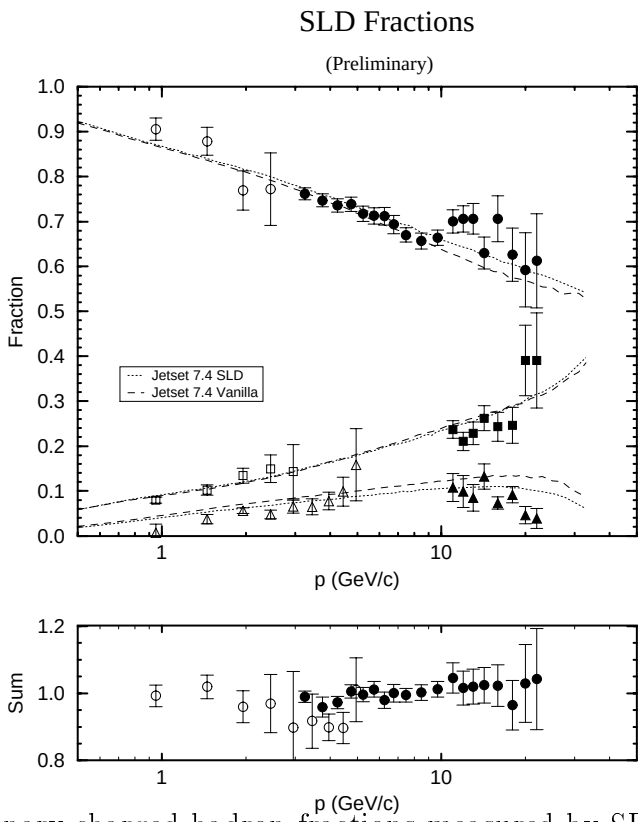

Fig. 14. Preliminary charged hadron fractions measured by SLD. Circles denote particles identified as $\pi^{\pm}$ (top points), squares are $K^{\pm}$ (middle points), and triangles are $p/\overline{p}$ (lower points). Open symbols are for the liquid radiator and solid symbols for the gas radiator. The lower figure shows the sum of the efficiencies, which should equal 1.0.

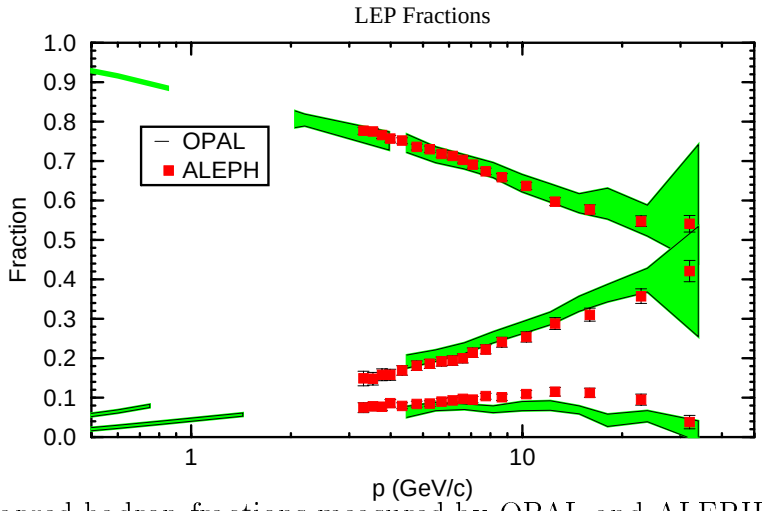

Fig. 15. Charged hadron fractions measured by OPAL and ALEPH using ionization loss techniques.

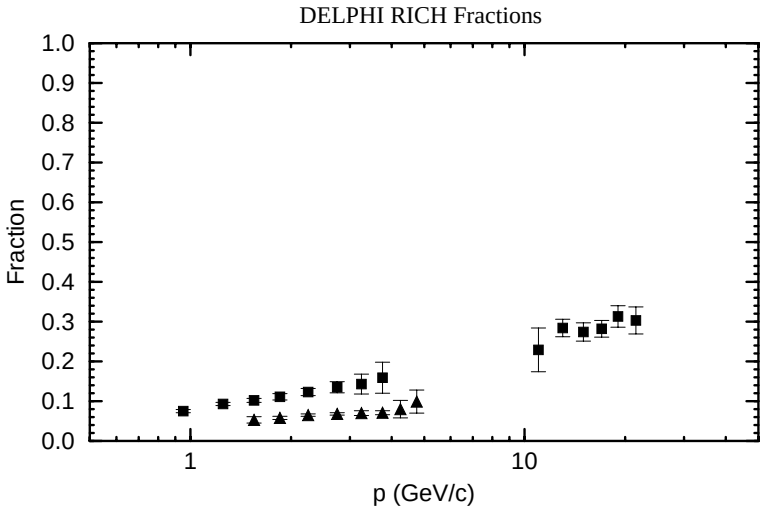

Fig. 16. Charged hadron fractions measured using the ring imaging technique in the DELPHI RICH.

Neutral strange particle production (Λ/K^0) was also measured starting with all well-measured pairs of oppositely charged particles in the barrel region ($|\cos\theta| < 0.80$). Other requirements included an acceptable vertex with fit probability greater than 2%, the V^0 momentum pointing back to the IP, and an e^+e^- invariant mass greater than 70 MeV. The kinematic overlap between Λ's and K^0 was eliminated using standard techniques.

Figure 17 shows the measured hadron fractions as a function of scaled momentum $x_p = 2p/W$ for the five measured species. Cross sections for the charged hadrons were obtained by multiplying the measured fractions by the total hadronic cross section generated by JETSET 7.4 (Ref. 24). Note that the cross sections for charged and neutral kaon production are consistent.

For comparison with QCD+LPHD predictions,[28] the analysis was repeated as a function of $\xi = \ln(1/x_p)$. The resulting spectra are shown in Fig. 18 and in general are adequately fit by Gaussians within the point-to-point errors. The peak positions are listed in the table.

Particle	ξ-Peak Position
$\pi^\pm$	$3.74 \pm 0.01 \pm 0.04$
K^0	$2.60 \pm 0.02 \pm 0.02$
$\Lambda\overline{\Lambda}$	$2.63 \pm 0.04 \pm 0.01$

This analysis was repeated on high-purity light (uds) and heavy (b) quark samples which were isolated as described in the section on multiplicity measurements.

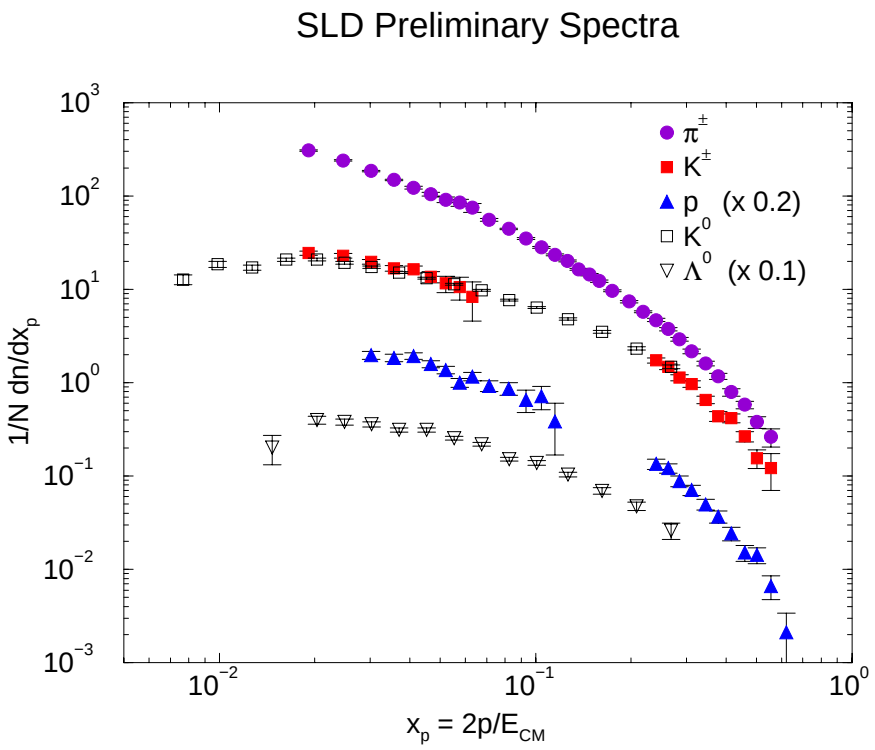

Fig. 17. Preliminary SLD spectra for five particle species as a function of $x_p = p/p_{beam}$. The $p/\overline{p}$ points are multiplied by 0.2 and the $\Lambda/\overline{\Lambda}$ points by 0.1 to make the figure clearer.

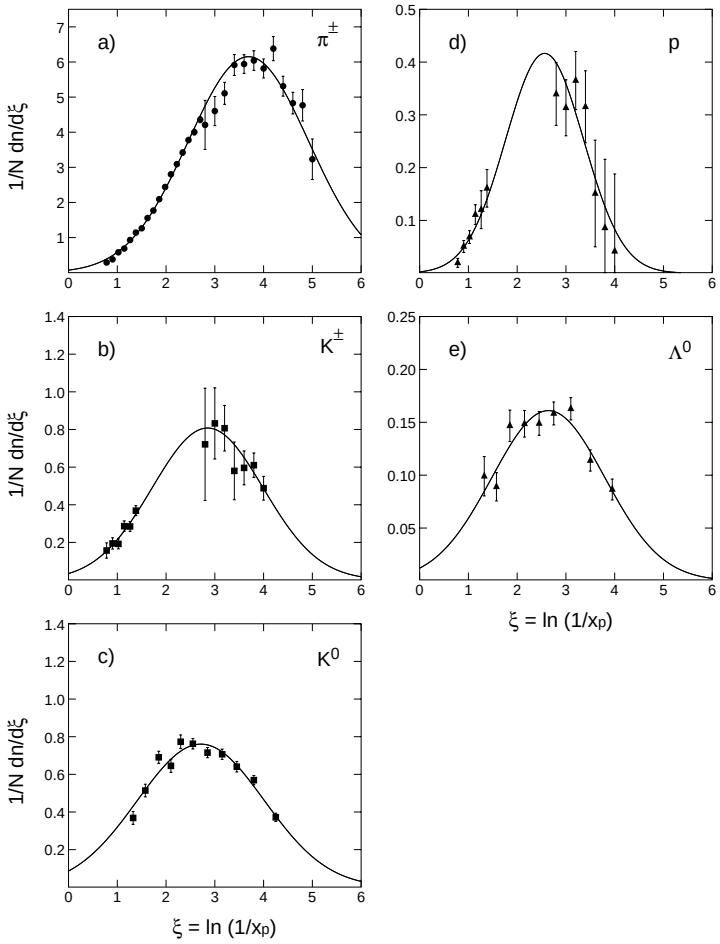

Fig. 18. Preliminary production spectra as a function of $\xi = -\ln x_p$. The curves are Gaussian fits. As in Fig. 17, the errors include systematic and statistical contributions added in quadrature. The systematic errors on the charged species are dominant and correlated point-to-point. An overall normalization uncertainty of 4% is not included.

The resulting spectra are shown in Fig. 19. Note the higher production of kaons and pions in the b-tagged sample and lower production of baryons. Except for the pion peak being lower in the b sample by 0.15 ± 0.05, there are no significant differences.

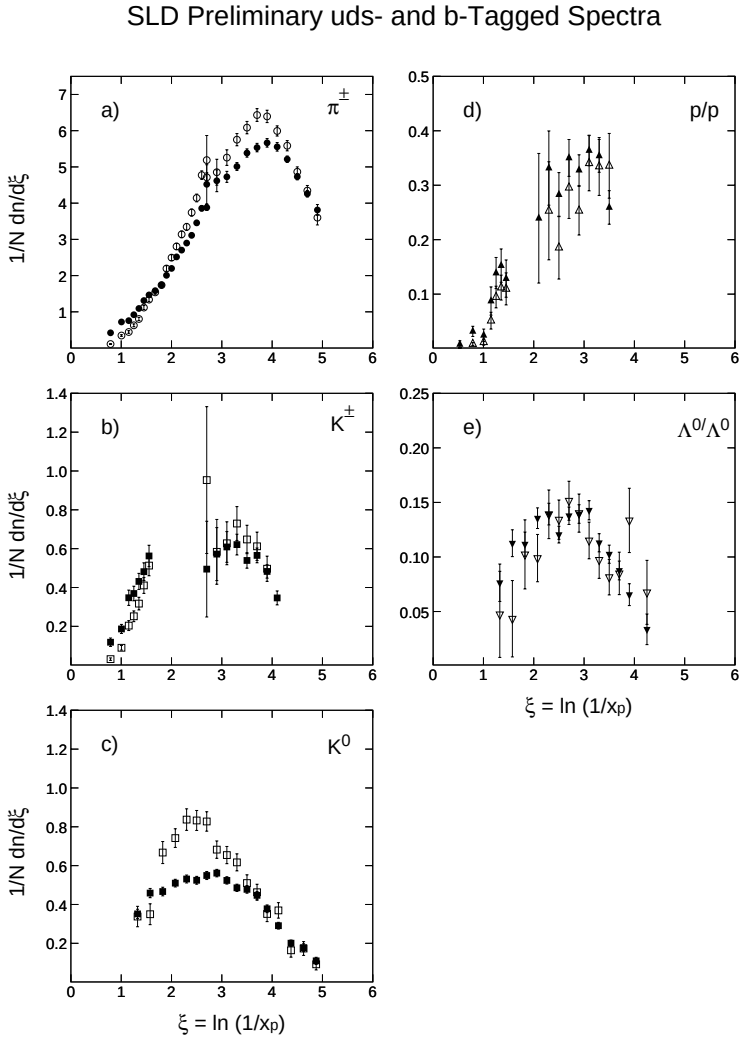

Fig. 19. Preliminary production spectra for samples enriched in $Z^0 \to u\overline{u}, d\overline{d}, s\overline{s}$ (solid symbols), and $Z^0 \to b\overline{b}$ (open symbols).

As a final exploitation of the beam polarization, an investigation was carried out to see if the quark forward-backward asymmetry relative to the beam polarization produces an observable leading-particle effect.

Figure 20 shows that fast Λ's and protons do indeed tend to follow the quark direction while fast $\overline{p}$'s and $\overline{\Lambda}$'s tend to follow the anti quark direction. The

average asymmetry for p > 10 GeV/c is 0.44 ± 0.07, thereby giving six standard deviations evidence for a leading-particle effect.

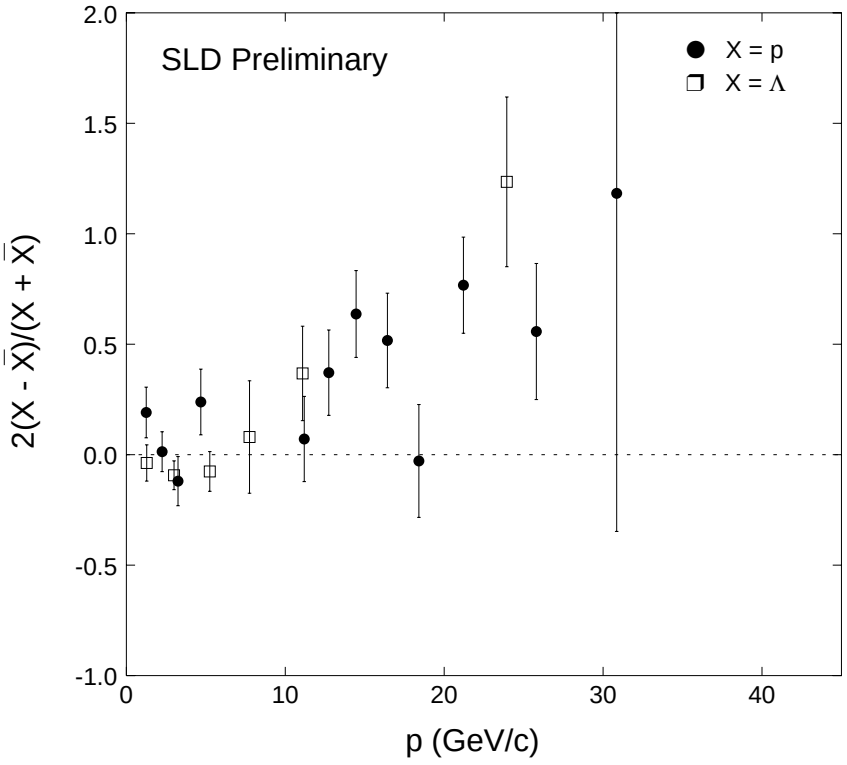

Fig. 20. The asymmetry between p, Λ, and their antiparticles in quark-tagged jets (those in the electron direction for left-handed electrons and in the opposite direction for right-handed beam polarization). Statistical errors only.

9 Summary

As should be clear from the results presented here, SLD is doing excellent QCD physics. In many cases, SLD is competitive or even superior to LEP in spite of the much higher statistics available to the LEP experiments.

Many of the results are limited by systematic errors, even at the statistics available to SLD. Since the systematics at SLC/SLD are quite different from those

at LEP, independent measurements are well worth doing. This is especially true because of the quality of the SLD detector and the unique features of SLC/SLD:

- Flavor selection using the number of significant impact parameters has been highly effective due to the tiny beam size, stable beam position, and precise vertex detector.
- Particle ID has shown high efficiency.
- The beam polarization has not only produced the best determination of $\sin^2\theta_W$, but has made possible the demonstration of a leading-particle effect associated with quark jets, and helped to show that other possible spin effects are not easily detectable.

The future looks promising, given success in meeting the following goals:

- A vertex detector with increased coverage, efficiency, and accuracy.
- Increased statistics, with continuing high beam polarization.
- Reliable operation of both SLC and SLD.

References

[1] K. Abe *et al.*, "Factorial and cumulant moments in $e^+e^- \to$ hadrons at the Z^0 resonance," SLAC-PUB-7027 (1996); to appear in Phys. Lett. B.

[2] K. Abe *et al.*, "Measurement of the charged multiplicities of b, c, and light quark events from Z^0 decays," SLAC-PUB-6924 (1995).

[3] K. Abe *et al.*, "First study of rapidity gaps in e^+e^- annihilation," SLAC-PUB-7076 (1996); to appear in Phys. Rev. Lett.

[4] K. Abe *et al.*, "A study of the orientation and energy partition of three-jet events in hadronic Z^0 decays," SLAC-PUB-6922 (1995).

[5] K. Abe *et al.*, "An improved limit on jet handedness in Z^0 decays," SLAC-PUB-6921 (1995).

[6] K. Abe *et al.*, "First measurement of the T-odd correlation between the Z^0 spin and the three-jet plane orientation in polarized Z^0 decays to three jets," Phys. Rev. Lett. **75**, 4173 (1995).

[7] K. Abe *et al.*, "Production of $\pi^{\pm}$, $K^{\pm}$, p, K^0, Λ in hadronic Z^0 decays," SLAC-PUB-6920 (1995).

[8] SLD Design Report, SLAC Report 273 (1984).

[9] K. Abe *et al.*, Nucl. Instrum. Methods A **288**, 288 (1990).

[10] G. Giacomelli, Int. J. Mod. Phys. A **5**, 223 (1990).

[11] Z. Koba, M. B. Nielsen, and P. Oleson, Nucl. Phys. B **240**, 317 (1972).

[12] I. M. Dremin, Phys. Lett. B **313**, 209 (1993).

[13] I. M. Dremin *et al.*, Phys. Lett. B **336**, 119 (1994).

[14] I. M. Dremin, Mod. Phys. Lett. A **8**, 2747 (1993).

[15] Y. L. Dokshitzer *et al.*, J. Phys. G **17**, 1481 (1991); *ibid* G **17**, 1602 (1991).

[16] V. A. Petrov and A. V. Kisselev, CERN-TH-7318-94 (1994).

[17] F. Abe *et al.*, Phys. Rev. Lett. **74**, 855 (1994).

[18] T. Ahmed *et al.*, Nucl. Phys. B **249**, 477 (1994).

[19] J. Bjorken *et al.*, Phys. Lett. B **286**, 153 (1992).

[20] TASSO Collaboration, R. Brandelik *et al.*, Phys. Lett. B **86**, 243 (1979); Mark II Collaboration, D. P. Barber *et al.*, Phys. Rev. Lett. **43**, 830 (1979);
PLUTO Collaboration, C. Berger *et al.*, Phys. Lett. B **86**, 418 (1979); JADE Collaboration, W. Bartel *et al.*, Phys. Lett. B **91**, 142 (1980).

[21] SLD Collaboration, K. Abe *et al.*, Phys. Rev. Lett. **74**, 1512 (1994).

[22] K. Fabricius *et al.*, Phys. Rev. Lett. **45**, 867 (1980), and J. G. Körner *et al.*, Phys. Lett. B **94**, 207 (1980).

[23] A. Brandenburg, L. Dixon, and Y. Shadmi, SLAC-PUB-95-6725, April 1995 (to be published in Phys. Rev. D, 1996).

[24] ALEPH Collaboration, D. Decamp *et al.*, Z. Phys. C **55**, 209 (1992).

[25] OPAL Collaboration, P. D. Acton *et al.*, Z. Phys. C **63**, 181 (1994).

[26] ALEPH Collaboration, D. Decamp *et al.*, CERN-PPE-94/201 (submitted to Z. Physics C).

[27] DELPHI Collaboration, P. Abreu *et al.*, CERN-PPE-95/28 (submitted to Nucl. Phys. B).

[28] T. I. Azimov, Y. L. Dokshitzer, V. A. Khoze, and S. I. Troyan, Z. Phys. C **27**, 65 (1985).